In Situ Method Correlating Raman Vibrational Characteristics to Chemical Expansion via Oxygen Nonstoichiometry of Perovskite Thin Films

*Eva Sediva, Thomas Defferriere, Nicola H. Perry, Harry L. Tuller, Jennifer L.M. Rupp**

E. Sediva [1,2], T. Defferriere [1], Prof. N. H. Perry [4,5], Prof. H. L. Tuller [1], Prof. J. L.M. Rupp [1,2,3*]

1 Department of Materials Science and Engineering, Massachusetts Institute of Technology, 77 Massachusetts Av., Cambridge MA, 02139, USA

2 ETHZ Department of Materials, Hönggerbergring 64, 8093, Zürich, Switzerland

3 Department of Electrical Engineering and Computer Science, Massachusetts Institute of Technology, 77 Massachusetts Av., Cambridge MA, 02139, USA

4 Department of Materials Science and Engineering and Materials Research Laboratory, University of Illinois at Urbana-Champaign, 1304 W. Green St., Urbana IL, 61801, USA

5 International Institute for Carbon-Neutral Energy Research (WPI-I2CNER), Kyushu University, 744 Motooka, Nishi-ku Fukuoka, 819-0395, Japan

*jrupp@mit.edu

Keywords: chemo-mechanical coupling, electrochemical titration, Raman spectroscopy, oxide perovskites

Effective integration of perovskite films into devices requires knowledge of their electro-chemo-mechanical properties. Raman spectroscopy is an excellent tool for probing such properties as the film's vibrational characteristics couple to the lattice volumetric changes during chemical expansion. While lattice volumetric changes are typically accessed by analyzing Raman shifts as a function of pressure, stress or temperature, such methods can be impractical for thin films and do not capture information on chemical expansion. Here we report an *in situ* Raman spectroscopy technique, using an electrochemical titration cell to change the oxygen nonstoichiometry of a model perovskite film, $Sr(Ti,Fe)O_{3-y}$, and correlate the lattice vibrational properties to the material's chemical expansion. We discuss how to select an appropriate Raman vibrational mode to track the evolution in oxygen nonstoichiometry. Subsequently, we

This is the author manuscript accepted for publication and has undergone full peer review but has not been through the copyediting, typesetting, pagination and proofreading process, which may lead to differences between this version and the Version of Record. Please cite this article as doi: 10.1002/adma.201902493.

track the frequency of the oxygen stretching mode around Fe^{4+}, as it decreases during reduction as the material expands and increases during re-oxidation as the material shrinks. This methodology of oxygen pumping and *in situ* Raman of oxide films enables future *in operando* measurements even for small material volumes, as typical for applications of films as electrodes or electrolytes utilized in electrochemical energy conversion or memory devices.

1. Introduction

Compositions of the perovskite oxide system $Sr(Ti,Fe)O_{3-y}$ are of interest as mixed ionic-electronic conductors in environmental oxygen sensing,[1] resistive switches for memories and computing [2–6] and solid oxide fuel cell electrodes for energy conversion.[7,8] For many of these applications, processing the material in thin film form, and at low temperatures suitable for silicon integration, is desirable. This requires control over the thin film structure-property relationships such as fast reaction kinetics, ionic and electronic conductivities,[1,9] stoichiometry,[10] optical transmittance [11] and/or mechanical properties.[12,13] The small sample volumes, large interfacial areas and substrate confinement of the thin films often result in substantially altered properties when compared to macroscopic bulk $Sr(Ti,Fe)O_{3-y}$ specimens, processed by powder pressing and sintering at higher temperatures.[14,15] For example, when processed as a thin film, $Sr(Ti,Fe)O_{3-y}$ reveals a higher optical transmittance [11] and lower conductivity, [9] e.g. in $SrTi_{0.65}Fe_{0.35}O_{3-y}$ [1] the latter by one order of magnitude. Additionally, $Sr(Ti,Fe)O_{3-y}$ shows strong coupling between electrical, chemical and mechanical properties, such as the connection between charge transport, oxygen nonstoichiometry and volumetric expansion, namely an *electro-chemo-mechanical* coupling; see Refs. [14–16] for details. It is important to characterize these coupling effects by *in situ* measurements of oxygen nonstoichiometry (chemical changes) simultaneously with electrical or mechanical thin film properties as they may ultimately define the endurance and performance of future resistive random access memory architectures for computing, or high volumetric density micro-fuel cells and sensing devices.

1.1 State-of-the-art of characterization and control of oxygen nonstoichiometry in thin films

Chemical oxygen nonstoichiometry changes in oxide thin films can be measured with the aid of Electrochemical Impedance Spectroscopy (EIS) by evaluating the chemical capacitance, by optical absorption or by piezocrystal microbalance, see summary in Figure 1a. In general, one can distinguish between “contact” (e.g. by EIS and piezocrystal) and “contactless” (e.g. by optical absorption) techniques, the latter of interest when metal contacts and current collectors, e.g. used during impedance spectroscopy measurements can influence, for example, the characterization of surface reaction kinetics.[11] Using a piezocrystal substrate, oxygen nonstoichiometry is measured by monitoring the mass change during an oxygen exchange experiment.[17,18] In such studies, however, the initial oxygen nonstoichiometry of the as-

deposited thin film is ordinarily unknown. Turning to the contactless methods, optical absorption measures the coupling of the optical transmittance with the valence state of a transition metal or rare earth ion in the lattice (e.g. in $Sr(Ti,Fe)O_{3-y}$, Fe^{3+}/Fe^{4+}) to access oxygen nonstoichiometry.[11] However the technique is indirect, requires calibration and there is no direct sensitivity to changes in mechanical volume. It has recently been demonstrated that it is possible to rapidly and precisely adjust the nonstoichiometry of $Sr(Ti,Fe)O_{3-y}$ and $(Pr,Ce)O_{2-y}$ thin films with the aid of an electrochemical titration cell, where oxygen is pumped in and out of the oxide film working electrode through an oxygen ion electrolyte controlled by a Nernst potential.[11,19] This has been successfully adapted for *in situ* optical absorption and mechanical actuation studies, see Refs. [11,20,21] for details.

All of the above-mentioned methods are limited in that additional techniques are needed to probe the mechanics, such as nano-indentation,[22] while measuring oxygen nonstoichiometry, in order to access the chemo-mechanical interactions of oxide thin films. Vibrational spectroscopy, on the other hand, would appear to be an ideal candidate for accessing chemo-mechanical interactions in thin films, given its sensitivity to materials expansion via the coupling between bond lengths and their vibrations.[23] We demonstrate the use of *in situ* Raman spectroscopy to capture chemo-mechanical coupling in $Sr(Ti,Fe)O_{3-y}$ thin films by monitoring their lattice vibrational properties while changing their oxygen nonstoichiometry. In the following, we review the defect chemical models of $Sr(Ti,Fe)O_{3-y}$ solid solutions and their coupling to chemical expansion.

1.2 Oxygen nonstoichiometry and chemical expansion in the $Sr(Ti,Fe)O_{3-y}$ solid solutions

$Sr(Ti,Fe)O_{3-y}$ solid solutions provide a convenient model system to study changes in oxygen nonstoichiometry given the stability of their cubic phase over large temperature and oxygen nonstoichiometry ranges. Reduction-induced chemical expansion in oxides refers to lattice dilation that accompanies a decrease in oxygen content. Analogous to the coefficient of thermal expansion (CTE), the coefficient of chemical expansion (CCE) is defined as [15]

$$\alpha_C = \pm \frac{\varepsilon_C}{\Delta\delta}, \quad (1)$$

where α_C is the chemical expansion coefficient, ε_C the induced isothermal chemical strain and $\Delta\delta$ the change in oxygen stoichiometry (per formula unit), with the sign positive for cases where δ represents oxygen deficiency (sub-stoichiometry) and negative for cases where δ represents oxygen excess (super-stoichiometry) relative to the reference compound (as in the present work). Chemical expansion in $Sr(Ti,Fe)O_{3-y}$ is driven by the reduction of iron from Fe^{4+} to Fe^{3+} and further to Fe^{2+}.[15] The increase in the iron ionic radius is the driver for lattice expansion, since the radius of the oxygen vacancy remains similar to the occupied oxygen anion site.[15] We refer here to the defect chemical model developed by Rothshild et al. who used $SrTi_{1-x}^{4+}Fe_x^{3+}O_{3-}$

$_{x/2+\delta}$ ($y = x/2+\delta$) as the reference state where δ is the oxygen nonstoichiometry.[14] The reference state takes into account, that Fe^{3+} is the prevailing oxidation state and δ increases as oxygen is introduced into the lattice and iron adopts the 4+ valence. We can express the oxygen nonstoichiometry in Kröger-Vink notation as: $\delta = ([O_i''] - [V_O^{\cdot\cdot}])/\left[SrTi_{1-x}Fe_xO_{3-y}\right]$. Here [$SrTi_{1-x}Fe_xO_{3-y}$] is the volumetric concentration of $Sr(Ti,Fe)O_{3-y}$ formula units and $[O_i'']$ and $[V_O^{\cdot\cdot}]$ refer to the concentrations of oxygen on "interstitial" sites (relative to the oxygen-deficient reference state) and oxygen vacancies.[15] In this case $\delta = x/2$ for oxidized conditions where all the iron adopts the 4+ state and $\delta = 0$ in the completely reduced reference state.

Perry et al. determined the chemical expansion coefficients as a function of temperature of macroscopic ceramic pellets of $Sr(Ti,Fe)O_{3-y}$ with 5 and 35 mol% Fe by coupled thermogravimetric and dilatometric analysis.[15] The relationship between chemical expansion and nonstoichiometry in thin films has not yet been quantified since thermogravimetric analysis and dilatometry are not suitable characterization methods given the small sample volumes and supporting substrate in thin films. *In situ* X-Ray diffraction can also be potentially used to quantifying film chemical expansion from lattice constant measurements,[24] however, the small sample volumes combined with the long-range averaging nature of X-Ray diffraction can limit the pattern intensity.

One way to overcome these challenges is by examining the *in situ* Raman spectroscopy of a film integrated onto an electrochemical oxygen pump. This has the potential to uncover the yet unknown coupling of the material's chemical expansion to the vibrational properties of the material.

1.3 In situ Raman Spectroscopy Using Electrochemical Cells to Probe Chemo-Mechanics of Perovskite Films

Conventionally, lattice volumetric changes can be probed with Raman spectroscopy by performing *in situ* thermal expansion [25] or high pressure contraction,[26–29] experiments, Figure 1b. Additionally in films, stress measurements using either the substrate curvature method [30] or film relaxation through substrate removal [31,32], Figure 1b, can reveal changes in bond lengths as a function of stress.

Raman spectra of $Sr(Ti,Fe)O_{3-y}$ solid solutions were measured and compared on completely oxidized ($\delta=x/2$) and reduced ($\delta=0$) powders. [33] In this study Vračar et al. showed that a new Raman mode around 690 cm^{-1} appears when Fe^{4+} is introduced into $SrTiO_3$ due to structural Jahn-Teller distortions around the Fe^{4+} ion. Their study motivated us to consider this Fe^{4+}-associated localized Raman band as a potential means for tracking the level of oxidation and coupled volumetric change in the ions' local environment. One would expect this to hold for both macroscopic pellets and thin films.

Through this work, we provide a methodology for measuring the chemical expansion of thin oxide films, and demonstrate that certain Raman active bands related to oxygen sublattice vibrations in perovskites can be used to quantify an oxide's oxygen nonstoichiometry. To date,

as far as we are aware, no *in situ* Raman experiments, measuring vibrational frequencies as a function of the degree of chemical expansion of oxide perovskite thin films, have previously been performed. In this study, we fill this gap by combining solid state electrochemical oxygen titration with Raman spectroscopy, Figure 1c. This enables precise control of the oxygen nonstoichiometry level over wide limits by electrochemically pumping oxygen in and out of the thin film while simultaneously measuring the Raman spectral characteristics. As a model perovskite system with a Jahn-Teller distortion upon oxidation, we select $Sr(Ti,Fe)O_{3-y}$ solid solutions and investigate, *in situ,* the correlation of oxygen nonstoichiometry vs. the Raman oxygen stretching mode frequency around Fe^{4+}.

Ultimately, it is shown that the oxygen nonstoichiometry, often difficult to determine in thin films with standard instrumentation, can be accessed via electrochemical pumping while simultaneously monitoring frequency shifts in the oxygen stretching peak of iron in the 4+ valence state via Raman spectroscopy. The quantitative relationship between the oxygen nonstoichiometry and Raman vibrational frequency enables us to determine a Raman chemical shift constant, analogous to the Grüneisen parameter describing the effects of chemical expansion on the Raman shift. Such studies have been predominantly accessed by pressure dependent Raman experiments on bulk materials in diamond anvil cells. This ability to probe small material volumes of perovskite films in a contactless manner opens new avenues to directly probe oxide films integrated within devices for various applications including photo- or electrochemical energy conversion cells or memristive devices for computer memories.

2. Experimental

2.1 Cell Fabrication

Platinum oxide was reactively sputtered (Kurt J. Lesker, Clairton, PA) on both sides of a single crystalline YSZ substrates (CrysTec, Germany) at a DC power of 50 W from a 99.99% pure Pt target (ACI Alloys) under 10 mTorr of 70% oxygen and 30% argon. [34] The resulting film thickness was 40 nm. The platinum oxide was subsequently reduced to porous platinum in the pulsed laser deposition (PLD) chamber at 650ºC under 0.027 mbar oxygen following the procedure outlined in Ref. [34]. A reference electrode was applied on the side of the YSZ substrate with silver paste.

The $SrTi_{1-x}Fe_xO_{3-y}$ PLD targets were prepared by a solid state synthesis including ball-milling, uniaxial and isostatic pressing and sintering powders at 1350ºC for 5 hours. The $SrTi_{1-x}Fe_xO_{3-y}$ thin films (x=0.3, 0.5) were deposited by pulsed laser deposition (Surface, Germany) using a KrF excimer laser with a 248 nm wavelength (Coherent, USA). The deposition parameters were 0.027 mbar of O_2, 650ºC, 3000 shots at 1.9 Jcm^{-1} and 8 cm distance between the target and substrate A blocking layer of 20 nm of MgO was sputtered (AJA International ATC-1800) on top of the $Sr(Ti,Fe)O_{3-y}$ thin film to reduce the surface exchange between the oxide thin film and the atmosphere. The sputtered MgO

film was prepared in an atmosphere of 10 mTorr of 10% oxygen and 90% of argon at a power level of 150 W from a MgO target.

2.2 Cell characterization and measurements

The X-Ray diffraction patterns of the thin films were measured with a the Rigaku SmartLab with a Cu K_α rotating anode source in a coupled scan and a rocking curve. Images of the cross sections of the devices were acquired on a Zeiss Merlin high resolution scanning electron microscope.

Chronoamperometry measurements (Gamry Instruments, Reference 600TM) of the electrochemical cells were performed in a Linkam HS600 stage under an oxygen atmosphere at 347ºC.

Raman spectra were taken with a confocal WITec alpha300 R Raman microscope (WITec, Germany) with the 457 nm (2.71 eV) excitation wavelength, laser power of 1.5 mW and grating of 1800 grooves/mm giving a spectral resolution of 0.53 cm^{-1}. A 50x long distance objective (Zeiss, Germany) with a numerical aperture (NA) of 0.7 was used for the laser focusing, giving an approximate laser spot size of 1 μm.

3. Results and Discussion

3.1 Fabrication of the electrochemical cells with the $Sr(Ti,Fe)O_{3-y}$ working electrode

Figure 2a depicts the fabricated electrochemical cell integrating a $Sr(Ti,Fe)O_{3-y}$ film. The stack consists of 40 nm of porous platinum counter electrode, 500 μm single crystal YSZ electrolyte, 40 nm of porous platinum digitated electrodes as current collector, 100 nm of $Sr(Ti,Fe)O_{3-y}$ (deposited by PLD) working electrode and 20 nm of MgO oxygen blocking layer. The voltages to pump oxygen in and out of the $Sr(Ti,Fe)O_{3-y}$ thin film were applied between the bottom porous Pt counter electrode and the porous Pt current collector. The reference electrode used to monitor the Nernst voltage being applied was placed on the side of the YSZ substrate with silver paste. The Raman laser was focused on the $Sr(Ti,Fe)O_{3-y}$ film above the porous Pt current collector. Two compositions of $Sr(Ti,Fe)O_{3-y}$ with 50 and 30 mol% Fe were considered to evaluate the effect of iron content on the chemical expansion.

The X-Ray diffraction patterns, Figure S1, reveal a (110) growth orientation of the films. The scanning electron microscope image in Figure 2c shows the cross section of the device with the $SrTi_{0.7}Fe_{0.3}O_{3-y}$ film in the role of the working electrode after electrochemical cycling. We can distinguish the individual layers of platinum, the $Sr(Ti,Fe)O_{3-y}$ film and the MgO capping layer. The 100 nm thick $Sr(Ti,Fe)O_{3-y}$ film is dense with a polycrystalline columnar microstructure characteristic of the pulsed laser deposition.

3.2 Raman spectra of the $Sr(Ti,Fe)O_{3-y}$ solid solutions for thin films without applied cell potentials

Before performing *in situ* electrochemical cycling, we measured the Raman spectra at room temperature to identify and assign the oxygen vibrational modes to be monitored during oxygen nonstoichiometry changes. Figure 3a summarizes the room temperature Raman spectra of an undoped $SrTiO_3$ thin film and the as-deposited thin films of $SrTi_{0.5}Fe_{0.5}O_{3-y}$ and $SrTi_{0.7}Fe_{0.3}O_{3-y}$ measured in air.

We first turn to undoped $SrTiO_3$ to understand the nature of the Raman active modes, and subsequently the role of iron doping. $SrTiO_3$ has at the Γ point of the Brillouin zone four T_{1u} modes and one silent T_{2u} mode. Three of the T_{1u} modes are infrared active, one is acoustic and none are Raman active. [35] Modes at 483, 539 and 784 cm^{-1} were measured, Figure 3a, in $SrTiO_3$. We assign these modes according to the literature to first order modes, namely the transverse and longitudinal optical modes of the T_{1u} symmetry. [36,37] These first order Raman modes of $SrTiO_3$ have been shown to appear in both polycrystalline and epitaxial thin films [36,38,39] without being Raman active. This can be due to the lowering of the lattice symmetry by strain, microstress or the presence of defects such as oxygen vacancies [40] or polar grain boundaries. [41] In addition, broad features in the ranges 200 to 450 cm^{-1} and 600 to 800 cm^{-1} are assigned to second-order scattering in $SrTiO_3$. [40,41] Second-order Raman scattering is a process involving two phonons with relaxed lattice symmetry selection rules. Next, we analyze the effect of adding iron into $SrTiO_3$ through the Raman spectra of the $Sr(Ti,Fe)O_{3-y}$ solid solutions, Figure 3a. Consistent with the $SrTiO_3$ cubic reference, we also observe the first order modes of the cubic lattice around 484 and 550 cm^{-1} and assign them according to the $SrTiO_3$ cubic reference to the transverse and longitudinal first order T_{1u} Raman modes. Importantly, another strong mode appears around 695 cm^{-1} in $SrTi_{0.7}Fe_{0.3}O_{3-y}$ and 675 cm^{-1} in $SrTi_{0.5}Fe_{0.5}O_{3-y}$. We attribute it to a local oxygen vibration around the Fe^{4+} ion, based on the analysis of the Raman spectra of $Sr(Ti,Fe)O_3$ powders by Vračar et al.. [33] Comparison of these spectra with those of the structurally related compounds $(La(Fe,Cr)O_3$ and $(La,Sr)(Mn,Fe)O_3)$ [42,43] and *ab initio* calculations of $Sr(Ti,Fe)O_{3-y}$ [44,45] suggest that this high frequency mode is a local A_{1g} oxygen stretching mode around the Fe cation, Figure 3b. This enhanced A_{1g} mode disappears in completely reduced $SrTi_{1-x}Fe_xO_{3-x/2}$, [33] the reason being that a Fe^{3+}-oxygen vacancy complex exhibits a zero phonon density of states in the range of 620-760 cm^{-1}. [46]

Summarizing, we have characterized and assigned Raman modes to the spectra of $Sr(Ti,Fe)O_{3-y}$ thin films. As discussed above, a key challenge for perovskite thin films is to be able to monitor changes in oxygen stoichiometry or equivalently the valence state of redox active cations. Here, we propose, motivated by these findings, that the oxygen breathing mode connected to Fe^{4+} can serve as a convenient marker to probe the local environment around Fe^{4+} and thereby the Fe redox state in $Sr(Ti,Fe)O_{3-y}$ solid solutions. To test this hypothesis, we turn to the electrochemical cells to pump oxygen in and out of the $Sr(Ti,Fe)O_{3-y}$ thin films while measuring their Raman spectra *in situ*.

3.3 In situ Raman measurements of the oxygen stretching mode in perovskite films and oxygen nonstoichiometry quantification

In an *in situ* experiment, the oxygen nonstoichiometry of the $Sr(Ti,Fe)O_{3-y}$ solid solutions was adjusted with the application of a DC bias in pure oxygen atmosphere while simultaneously measuring the Raman spectra. Measurements were performed at 347ºC to assure sufficient oxygen mobility in the electrolyte. The effective partial pressure of oxygen in the $Sr(Ti,Fe)O_{3-y}$ thin film is governed by the Nernst equation, Figure 2b.

$$p_{O_2,eff} = p_{O_2,gas} exp\left(\frac{4e\Delta E}{k_B T}\right) \quad (2)$$

Here ΔE is the applied bias, e the elementary charge, T the temperature, k_B the Boltzmann constant and $p_{O_2,gas}$ the oxygen partial pressure in the surrounding atmosphere. With a positive applied bias, oxygen is pumped through the electrolyte into the working electrode thin film, which is oxidized. The opposite occurs upon application of a negative bias, leading to reduction of the film.

First, the reduced state of $SrTi_{1-x}^{4+}Fe_x^{3+}O_{3-x/2+\delta}$ ($y = x/2+\delta$) with $\delta \approx 0$ was accessed by applying a negative voltage until the enhanced oxygen stretching mode associated with Fe^{4+} disappeared. The required voltages were -0.45 V for $SrTi_{0.7}Fe_{0.3}O_{3-y}$ and -0.35 V for $SrTi_{0.5}Fe_{0.5}O_{3-y}$ and they were applied for 40 minutes. The respective Raman spectra are shown in Figure S2. Subsequently more positive voltages were applied to pump oxygen into the film to partially oxidize it and thereby access intermediate oxygen nonstoichiometry levels, see Figure 4a and Figure S3.

The quantification of oxygen entering the perovskite film is achieved by measuring the integrated current (charge) passing through the electrochemical cell during the application of the Nernst voltage. [47] The current vs. time curve upon accessing the reference stoichiometric state with -0.35 V is plotted in Figure 4b for the as-deposited $SrTi_{0.5}Fe_{0.5}O_{3-y}$ thin film. We observe a large initial (negative) current increase that decays with time as the material reaches its equilibrium state at this voltage level. The negative current signifies that oxygen is being pumped out of the thin film, leading to a change in iron valence from 4+ to 3+. For the calculation of the oxygen nonstoichiometry, we assume here that all the iron is at this point in the 3+ valence state, but there can be residues of Fe^{4+} and even progressive reduction to Fe^{2+}. The subsequent partial oxidation with respect to the reduced reference at -0.15 V is shown in Figure 4c, where a similar current decay over time is observed. Positive currents are observed here since oxygen is being pumped into the reduced $SrTi_{0.5}Fe_{0.5}O_{3-y}$ film. The current evolution for all the applied voltages is summarized in Figure S4. In the next step the oxygen nonstoichiometry of the oxide was estimated by integrating the current-time curve, which is

schematically indicated by the hatched gray region in Figure 4c. The oxygen nonstoichiometry then becomes

$$\delta = \frac{a^3}{2eV_{film}} \int I(t)dt. \quad (3)$$

Here e is the elementary charge, V_{film} is the volume of the $SrTi_{1-x}Fe_xO_{3-y}$ thin film, $I(t)$ is the current as a function of time and a^3 is the volume of the $Sr(Ti,Fe)O_{3-y}$ unit cell. In general, the contributions to the current are the leakage of oxygen ions from the top interface into the surrounding gas (in blue) and the oxygen ions pumped through the YSZ electrolyte into the film (hatched gray region), see Figure 4c. We confirm that the electrochemical cell at 347 ºC is suitable for pumping oxygen in and out of the $Sr(Ti,Fe)O_{3-y}$ thin film, as leakage currents stay relatively low below 0.15 µA for all conditions, compared to the initial pumping current above 8 µA. This insures that oxygen surface exchange with the atmosphere can be effectively ignored and that the film stoichiometry can be fixed by measuring total Faradaic charge passed.

In the insets of Figure 4b,c we plot the respective Raman spectra obtained for the reduction condition at -0.35 V and the subsequent partial oxidation at -0.15 V. We see that the enhanced oxygen stretching mode disappears during oxidation as expected from previous reports [33,46] (on a side note, the substrate peak of YSZ appears around 600 cm^{-1}).

In this section we demonstrated that the electrochemical cell set-up enables the quantification of the oxygen nonstoichiometry during cell operation from the current vs. time curves analyzing the charge entering or leaving the $Sr(Ti,Fe)O_{3-y}$ thin film. Next we correlate the results of the *in situ* Raman spectroscopy with the calculated oxygen nonstoichiomtery.

3.4 In situ Raman spectroscopy as a function of $Sr(Ti,Fe)O_{3-y}$ oxygen nonstoichiometry accessed by electrochemical pumping of oxygen

The resulting oxygen nonstoichiometry and the oxygen breathing Raman mode positions as a function of applied bias are shown in Figure 5a and b for 30 and 50 mol% Fe respectively. We first discuss the trend in the oxygen nonstoichiometry as a function of applied bias. The oxygen nonstoichiometry δ, indicating larger oxygen contents, increases with applied bias. We report the final nonstoichiometries of 0.147±0.021 and 0.187±0.020 for 30 and 50 mol% Fe respectively for an applied voltage of 0.15 V, indicating close to full oxidation with 30 and partial and progressive oxidation with 50 mol% Fe. For a comparison with literature results on bulk $SrTi_{0.65}Fe_{0.35}O_{3-y}$ and a discussion on the experimental errors see also Figure S5 and Section 5 in the Supporting Information.

The Raman spectra at each applied bias, Figure S6, were fitted with a Lorentzian function, and the oxygen stretching mode frequency, Figure 5a and b, and amplitude, Figure S7, were followed. The fitted curves are shown in Figure S8. In both compositions the frequency of the oxygen stretching mode increases with applied voltage, meaning the mode hardens with oxidation of the $Sr(Ti,Fe)O_{3-y}$ thin film. This is consistent with an expected contraction of the lattice and shortening of the Fe-O bonds upon oxidation and increasing Fe^{4+} content. The overall change in the frequency between the lowest and highest applied bias is 13.8±1.9 cm^{-1} and 29.7±1.0 cm^{-1} for 30 and 50 mol% Fe. The higher frequency change with higher levels of iron is expected as iron is the mixed valence cation responsible for the oxygen nonstoichiometry changes and the accompanied lattice expansion or contraction. At the highest oxygen nonstoichiometry values, the Raman mode reaches 697.6±1.0 cm^{-1} for 30 and 694.3±0.7 cm^{-1} for 50 mol% Fe. This is in agreement with a previous Raman study on completely oxidized $Sr(Ti,Fe)O_3$ powders, [33] where the frequency of the enhanced mode ascribed to a local oxygen stretching around Fe^{4+} activated by the Jahn-Teller distortion was between 690 and 695 cm^{-1} for all considered compositions.

Next we can directly compare the two different iron compositions with respect to their Raman mode shifts as a function of oxygen nonstoichiometry, Figure 5c. We analyze the slopes $(\partial\nu/\partial\delta)_{T,P}$ from linear fits, Figure 5c, giving 123±24 and 180±25 cm^{-1} for 30 and 50 mol% Fe respectively. Here ω is the Raman mode frequency, δ the oxygen nonstoichiometry and the T, P indexes signify the constant pressure and temperature during the experiment. We'd like to point out, that the relationship between the Raman frequency and oxygen nonstoichiometry in Figure 5c can be a higher order than linearity. However, the reproducibility and volume measurement errors (see Supporting Information Section 5) do not allow a more precise analysis.

3.5 Quantification of the contribution of chemical expansion to the Raman shift

The vibrational frequency dependence on pure, isotropic, volumetric lattice changes in a material is usually described by the Grüneinsen parameter $\gamma_i = -\partial \ln \nu_i / \partial \ln V$, where the index *i* specifies the vibrational mode, *V* is the sample volume and ω_i the vibrational mode frequency. Volumetric changes during chemical expansion are often accompanied by a local symmetry change when the redox state of the metal cation changes. In the case of $Sr(Ti,Fe)O_{3-y}$, we are tracking frequency changes of a single mode around Fe^{4+} that does not change symmetry. However, locally, around the Fe^{4+} the Jahn-Teller distortion relaxes, when iron acquires the 3+ oxidation state and the enhanced oxygen stretching mode disappears. This signifies both a symmetry break and local anisotropic expansion. By thermodynamic definition, this violates the existing constraint of a pure volume change (quasi-harmonic reversible conditions) that defines the Grüneinsen parameter. Consequently, one cannot directly use the Grüneinsen parameter definition in the case of chemical expansion. As a consequence, we aim in the following to calculate an analogue to the Grüneisen parameter describing contributions of chemical

expansion to the Raman shift, which can help to estimate volumetric changes in materials from Raman frequency data being aware of the local structural asymmetries created (see also Section 9 of the Supporting Information). We define the parameter as the Raman chemical shift constant

$$\gamma_{Ci} = \frac{1}{\nu_0 \beta_C}\left(\frac{\partial \nu_i}{\partial \delta}\right)_{T,P} \quad (4)$$

where δ is the oxygen nonstoichiometry, ν_0 the vibrational frequency at standard conditions, i represents the vibrational mode and β_c is the chemical expansivity [48–50] defined as

$$\beta_C = 1/V\left(\frac{\partial V}{\partial \delta}\right)_{T,P} \quad (5)$$

We take ν_0 to be the frequency close to the stoichiometric reduced $SrTi_{1-x}Fe_xO_{3-x/2}$ and $(\partial \nu/\partial \delta)_{T,P}$ the slope from Figure 5c. We estimate the chemical expansivity from experimentally measured chemical expansion coefficients of $SrTi_{0.65}Fe_{0.35}O_{2.825+\delta}$ by Perry et al. [15] as $\beta_C \approx 3\Delta\varepsilon_C/\Delta\delta = 3\alpha_C$, [49] where ε_C is the chemical strain measured from dilatometry and α_C is the chemical expansion coefficient, giving at 347ºC $\beta_C \approx 0.088$. Using these values, the Raman chemical shift constant is then calculated to be γ_C=2.05±0.38 for $SrTi_{0.7}Fe_{0.3}O_{3-y}$.

In the following we discuss the applicability of the above calculation to the specific case of electrochemical oxygen pumping into $Sr(Ti,Fe)O_{3-y}$ thin films. Firstly, the chemical expansivity used in Eq. 4 relies on measurements of bulk samples with a slightly larger iron content (x=0.35 vs x=0.30) and therefore can be an imprecise estimate for the current experiment. Secondly, the chemical strain in the thin film may be non-uniform depending on the distance from the substrate. Lastly, thin films are constrained by their substrates and cannot expand isotropically in all three directions. This leads to an overestimation of the expansivity, since the $\beta_C \approx 3\alpha_C$ holds only in cases of isotropic expansion. The films can, however, be partially or fully compensated for in the out of plane expansion,[13] Figure 6b.

Next, we use the calculated Raman chemical shift constant to estimate the expected volumetric changes during chemical expansion as a validation of our calculation. The expected Raman shift due to volumetric changes in the lattice follows [51]

$$\Delta\nu = -3\gamma_C\nu_0\frac{\Delta a}{a_0}, \quad (6)$$

where v_0 is the reference vibrational frequency, Δa is the change in the lattice constant and a_0 is the reference lattice constant. Using the experimental results of Vračar et al.,[33] Eq. 6 gives a frequency shift of 18.3±3.4 for the 30 mol% Fe composition. This is in excellent agreement to the Raman shift measured with the electrochemical pumping method, which is 18.4±4.2 cm^{-1} when extrapolating to the full oxygen nonstoichiometry window ($0<\delta<0.15$). This finding suggests that, in the $SrTi_{0.7}Fe_{0.3}O_{3-y}$ thin films, the Raman mode shift is primarily driven by chemical expansion, and the corresponding change in the lattice parameter. The Raman chemical shift constant therefore enables us to estimate volumetric lattice changes upon chemical expansion by measuring the Raman frequency shifts.

In $SrTi_{0.5}Fe_{0.5}O_{3-y}$ the application of Eq. 6 predicts a 20.3±10.0 cm^{-1} smaller Raman shift than measured in the *in situ* experiment. The possible reasons for the discrepancy between the measured Raman shifts and the experimental lattice constants are further discussed in Section 10 of the Supporting Information.

The *in situ* Raman experiment is schematically summarized in Figure 6. The volumetric changes in the thin film are driven by the reduction and oxidation of the transition metal iron cation highlighted on the lattice level in Figure 6a. This drives the thin film expansion during reduction, Figure 6b, that is coupled to the oxygen nonstoichiometry, bond length and finally vibrational frequency of the oxygen stretching mode accessible by Raman spectroscopy. The Raman spectra as a function of oxygen nonstoichiometry are plotted for $SrTi_{0.7}Fe_{0.3}O_{3-y}$ in Figure 6c.

4. Conclusion

Raman spectroscopy is an excellent technique for determining subtle lattice volumetric changes in materials. This advantage has been widely utilized in temperature, pressure or strain dependent *in situ* Raman experiments. However, *in situ* experiments studying the volumetric changes related to chemical expansion using Raman spectroscopy are still missing, in particular, for oxides in thin film form.

In this study of $Sr(Ti,Fe)O_{3-y}$ films, we present an *in situ* Raman spectroscopy method utilizing an electrochemical titration cell to reversibly change oxygen nonstoichiometry and quantify the lattice vibrational properties coupled to the material's chemical expansion capturing the *chemo-mechanical* coupling of the lattice. In the electrochemical titration cell various compositions of the $Sr(Ti,Fe)O_{3-y}$ solid solutions act as the working electrode and their Raman spectra are recorded *in situ* under an applied voltage. The position of the Raman oxygen stretching mode around the perovskite's transition metal ion Fe^{4+} was followed as a signature of the material's extent of oxidation. We extend previous *ex situ* reports on Raman spectroscopy of $Sr(Ti,Fe)O_{3-y}$, that revealed the existence of a Jahn-Teller activated Fe^{4+} oxygen stretching band, but did not

access the full oxygen nonstoichiomtery window *in situ*. We envision this method being applied to wider class of perovskites and other metal oxide materials to investigate their chemo-mechanical properties of potential importance as they are employed, for example, as thin film electrodes or electrolytes in chip-sized devices such as micro-energy convertors or memristive computation.

Supporting Information

Supporting Information is available from the Wiley Online Library or from the author.

Acknowledgements

The authors thank the reviewers for their useful editing of the initial versions of the manuscript. The authors would like to thank Chang Sub Kim for helpful advice about oxygen pumping experiments and Charles Settens for help with the X-Ray diffraction experiments. This work is supported by the Swiss National Science Foundation Starting Grant, grant number BSSGI0_155986 / 1. T. Defferriere and H.L. Tuller acknowledge US-DOE Basic Energy Sciences, Grant No. DE-SC0002633 for financial support under this program. This work made use of the MRSEC Shared Experimental Facilities at MIT, supported by the National Science Foundation under award number DMR-14-19807.

Conflict of Interest

The authors declare no conflict of interest.

Received: ((will be filled in by the editorial staff))
Revised: ((will be filled in by the editorial staff))
Published online: ((will be filled in by the editorial staff))

References

[1] S. J. Litzelman, A. Rothschild, H. L. Tuller, *Sens. Actuators B Chem.* **2005**, *108*, 231.

[2] M. Kubicek, S. Taibl, E. Navickas, H. Hutter, G. Fafilek, J. Fleig, *J. Electroceramics* **2017**, *39*, 197.

[3] R. Muenstermann, T. Menke, R. Dittmann, R. Waser, *Adv. Mater.* **2010**, *22*, 4819.

[4] M. Kubicek, R. Schmitt, F. Messerschmitt, J. L. M. Rupp, *ACS Nano* **2015**, *9*, 10737.

[5] F. Messerschmitt, M. Kubicek, S. Schweiger, J. L. M. Rupp, *Adv. Funct. Mater.* **2014**, *24*, 7448.

[6] E. Sediva, W. J. Bowman, J. C. Gonzalez-Rosillo, J. L. M. Rupp, *Adv. Electron. Mater.* **n.d.**, *0*, 1800566.

[7] W. Jung, H. L. Tuller, *Energy Env. Sci* **2012**, *5*, 5370.

[8] A. Nenning, L. Volgger, E. Miller, L. V. Mogni, S. Barnett, J. Fleig, *J. Electrochem. Soc.* **2017**, *164*, F364.

[9] S. Taibl, G. Fafilek, J. Fleig, *Nanoscale* **2016**, *8*, 13954.

[10] T. Kawada, J. Suzuki, M. Sase, A. Kaimai, K. Yashiro, Y. Nigara, J. Mizusaki, K. Kawamura, H. Yugami, *J. Electrochem. Soc.* **2002**, *149*, E252.

[11] N. H. Perry, J. J. Kim, H. L. Tuller, *Sci. Technol. Adv. Mater.* **2018**, *19*, 130.

[12] S. R. Bishop, D. Marrocchelli, C. Chatzichristodoulou, N. H. Perry, M. B. Mogensen, H. L. Tuller, E. D. Wachsman, *Annu. Rev. Mater. Res.* **2014**, *44*, 205.

[13] J. G. Swallow, J. K. Lee, T. Defferriere, G. M. Hughes, S. N. Raja, H. L. Tuller, J. H. Warner, K. J. Van Vliet, *ACS Nano* **2018**, *12*, 1359.

[14] A. Rothschild, W. Menesklou, H. L. Tuller, E. Ivers-Tiffe, *Chem. Mater.* **2006**, *18*, 3651.

[15] N. H. Perry, J. Jin Kim, S. R. Bishop, H. L. Tuller, *J. Mater. Chem. A* **2015**, *3*, 3602.

[16] N. H. Perry, D. Marrocchelli, S. R. Bishop, H. L. Tuller, *ECS Trans.* **2016**, *72*, 1.

[17] P. Simons, H.-I. Ji, T. C. Davenport, S. M. Haile, *J. Am. Ceram. Soc.* **2017**, *100*, 1161.

[18] S. Schröder, H. Fritze, S. Bishop, D. Chen, H. L. Tuller, *Appl. Phys. Lett.* **2018**, *112*, 213502.

[19] D. Chen, H. L. Tuller, *Adv. Funct. Mater.* **2014**, *24*, 7638.

[20] J. G. Swallow, J. J. Kim, J. M. Maloney, D. Chen, J. F. Smith, S. R. Bishop, H. L. Tuller, K. J. V. Vliet, *Nat. Mater.* **2017**, *16*, 749.

[21] N. H. Perry, N. Kim, E. Ertekin, H. L. Tuller, *Chem. Mater.* **2019**, *31*, 1030.

[22] J. G. Swallow, J. J. Kim, M. Kabir, J. F. Smith, H. L. Tuller, S. R. Bishop, K. J. Van Vliet, *Acta Mater.* **2016**, *105*, 16.

[23] R. Schmitt, J. Spring, R. Korobko, J. L. M. Rupp, *ACS Nano* **2017**, *11*, 8881.

[24] M. D. Biegalski, E. Crumlin, A. Belianinov, E. Mutoro, Y. Shao-Horn, S. V. Kalinin, *Appl. Phys. Lett.* **2014**, *104*, 161910.

[25] R. Cuscó, E. Alarcón-Lladó, J. Ibáñez, L. Artús, J. Jiménez, B. Wang, M. J. Callahan, *Phys. Rev. B* **2007**, *75*, 165202.

[26] A. F. Goncharov, V. V. Struzhkin, *J. Raman Spectrosc.* **2003**, *34*, 532.

[27] B. A. Weinstein, G. J. Piermarini, *Phys. Rev. B* **1975**, *12*, 1172.

[28] P. Perlin, C. Jauberthie-Carillon, J. P. Itie, A. San Miguel, I. Grzegory, A. Polian, *Phys. Rev. B* **1992**, *45*, 83.

[29] M. Ahart, M. Somayazulu, R. E. Cohen, P. Ganesh, P. Dera, H. Mao, R. J. Hemley, Y. Ren, P. Liermann, Z. Wu, *Nature* **2008**, *451*, 545.

[30] H. Li, P. Zhang, G. Li, J. Lu, Q. Wu, Y. Gu, *J. Alloys Compd.* **2016**, *682*, 132.

[31] Y. Shi, A. H. Bork, S. Schweiger, J. L. M. Rupp, *Nat. Mater.* **2015**, *14*, 721.

[32] O. Kraynis, E. Makagon, E. Mishuk, M. Hartstein, E. Wachtel, I. Lubomirsky, T. Livneh, *Adv. Funct. Mater.* **2019**, 1804433.

[33] M. Vracar, A. Kuzmin, R. Merkle, J. Purans, E. A. Kotomin, J. Maier, O. Mathon, *Phys. Rev. B* **2007**, *76*, 174107.

[34] W. Jung, J. J. Kim, H. L. Tuller, *J. Power Sources* **2015**, *275*, 860.

[35] R. A. Evarestov, E. Blokhin, D. Gryaznov, E. A. Kotomin, J. Maier, *Phys. Rev. B* **2011**, *83*, 134108.

[36] A. A. Sirenko, I. A. Akimov, J. R. Fox, A. M. Clark, H.-C. Li, W. Si, X. X. Xi, *Phys. Rev. Lett.* **1999**, *82*, 4500.

[37] J. D. Axe, *Phys. Rev.* **1967**, *157*, 429.

[38] V. I. Merkulov, J. R. Fox, H.-C. Li, W. Si, A. A. Sirenko, X. X. Xi, *Appl. Phys. Lett.* **1998**, *72*, 3291.

[39] S. Gupta, R. S. Katiyar, *J. Raman Spectrosc.* **2001**, *32*, 885.

[40] D. A. Tenne, I. E. Gonenli, A. Soukiassian, D. G. Schlom, S. M. Nakhmanson, K. M. Rabe, X. X. Xi, *Phys. Rev. B* **2007**, *76*, 024303.

[41] T. Ostapchuk, J. Petzelt, V. Železnỳ, A. Pashkin, J. Pokornỳ, I. Drbohlav, R. Kužel, D. Rafaja, B. P. Gorshunov, M. Dressel, et al, *Phys. Rev. B* **2002**, *66*, 235406.

[42] J. Andreasson, J. Holmlund, C. S. Knee, M. Käll, L. Börjesson, S. Naler, J. Bäckström, M. Rübhausen, A. K. Azad, S.-G. Eriksson, *Phys. Rev. B* **2007**, *75*, 104302.

[43] A. Dubroka, J. Humlíček, M. V. Abrashev, Z. V. Popović, F. Sapiña, A. Cantarero, *Phys. Rev. B* **2006**, *73*, 224401.

[44] E. Blokhin, E. A. Kotomin, J. Maier, *J. Phys. Condens. Matter* **2012**, *24*, 104024.

[45] R. Evarestov, E. Blokhin, D. Gryaznov, E. A. Kotomin, R. Merkle, J. Maier, *Phys. Rev. B* **2012**, *85*, 174303.

[46] E. Blokhin, E. Kotomin, A. Kuzmin, J. Purans, R. Evarestov, J. Maier, *Appl. Phys. Lett.* **2013**, *102*, 112913.

[47] G. Walch, B. Rotter, G. C. Brunauer, E. Esmaeili, A. K. Opitz, M. Kubicek, J. Summhammer, K. Ponweiser, J. Fleig, *J. Mater. Chem. A* **2017**, *5*, 1637.

[48] S. B. Adler, *J. Am. Ceram. Soc.* **2001**, *84*, 2117.

[49] Chen, Yu, S. B. Adler, *Chem. Mater.* **2005**, *17*, 4537.

[50] Y.-M. Kim, J. He, M. D. Biegalski, H. Ambaye, V. Lauter, H. M. Christen, S. T. Pantelides, S. J. Pennycook, S. V. Kalinin, A. Y. Borisevich, *Nat. Mater.* **2012**, *11*, 888.

[51] J. R. McBride, K. C. Hass, B. D. Poindexter, W. H. Weber, *J. Appl. Phys.* **1994**, *76*, 2435.

5. Figures

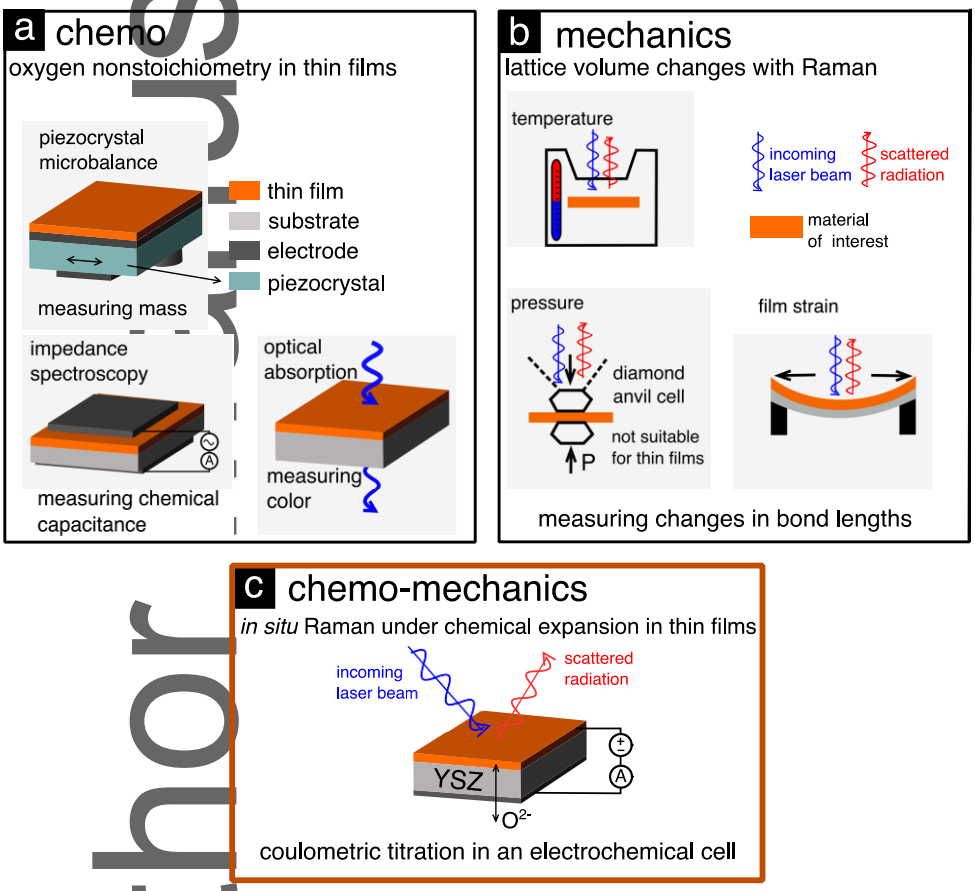

Figure 1: a. Summary of several methods used to measure oxygen nonstoichiometry in thin films. b. Experimental Raman spectroscopy methods for measuring materials lattice volumetric changes. c. Current experiment that combines measurement of materials expansion and contraction due to oxygen release and uptake.

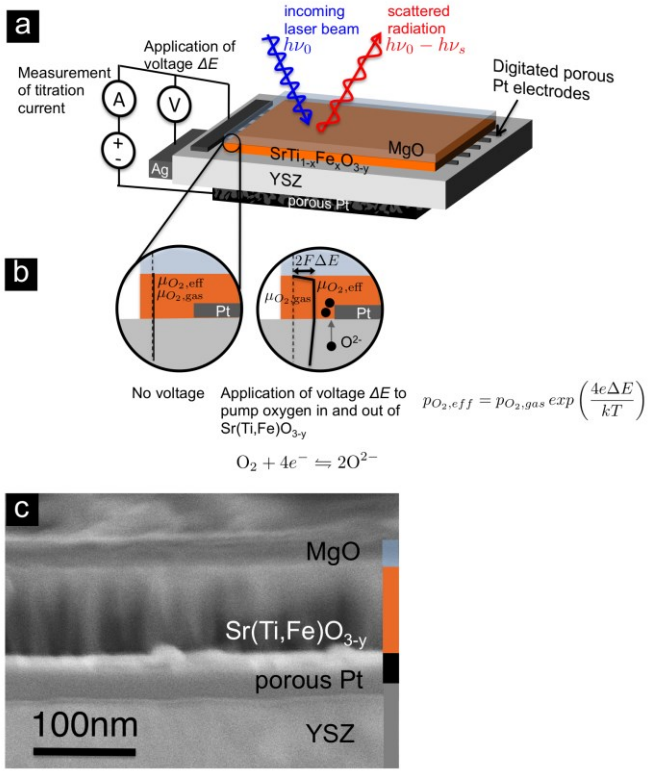

Figure 2: a. A schematic representation of the electrochemical cell consisting of a 40 nm porous Pt counter electrode, 500 µm YSZ electrolyte, 40 nm porous Pt layer, 100 nm of $Sr(Ti,Fe)O_{3-y}$ working electrode covered with 20 nm of MgO. The reference electrode was attached to the side of the YSZ substrate with silver paste. $h\upsilon_0$ is the incoming Raman excitation light energy and $h\upsilon_0$-$h\upsilon_s$ is the scattered light energy. b. A zoom into the electrolyte-electrode interface exemplifying the pumping mechanism. The bold solid line represents the effective chemical potential of oxygen as induced by an applied bias while the dashed line represents the reference gas phase chemical potential. c. An example high resolution scanning electron microscope image of the device cross-section after cycling.

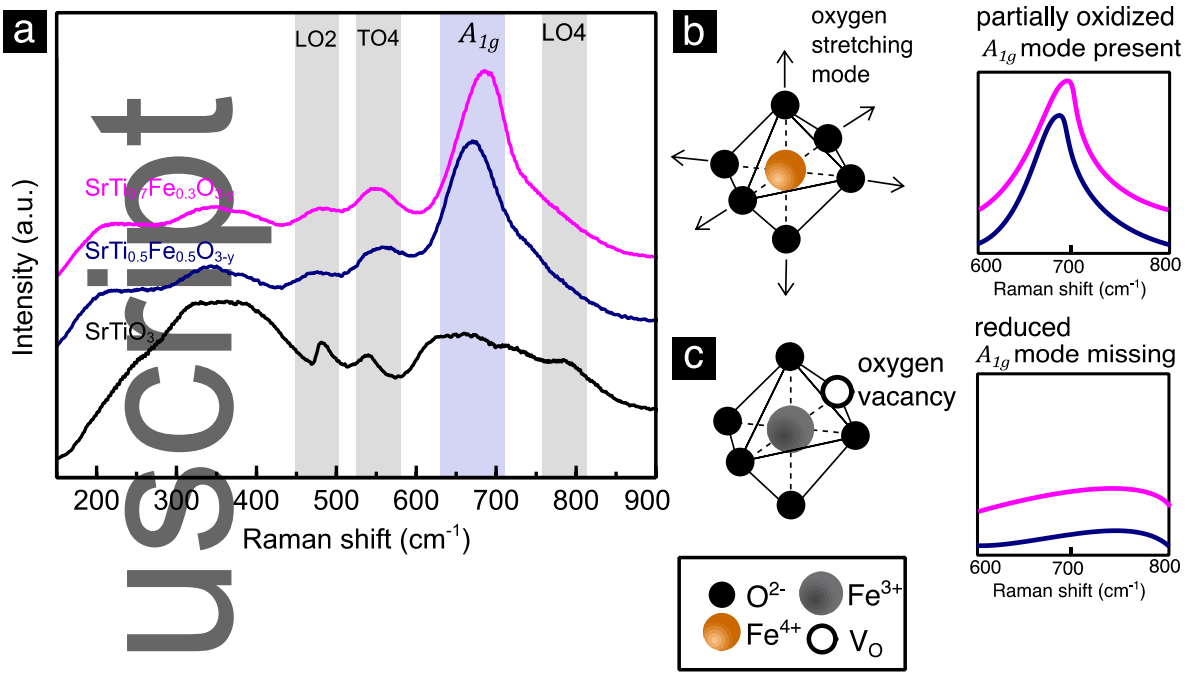

Figure 3: a. Raman spectra of the as-deposited $Sr(Ti,Fe)O_{3-y}$ thin films with 30 and 50 mol% Fe and a spectrum of a pure $SrTiO_{3-\delta}$ thin film taken at room temperature. All the spectra are normalized and shifted for clarity. b. Schematic of the oxygen vibrational mode around 690 cm^{-1} associated to Fe^{4+}. c. This oxygen stretching mode is missing in the Raman spectrum in the case of Fe^{3+}.

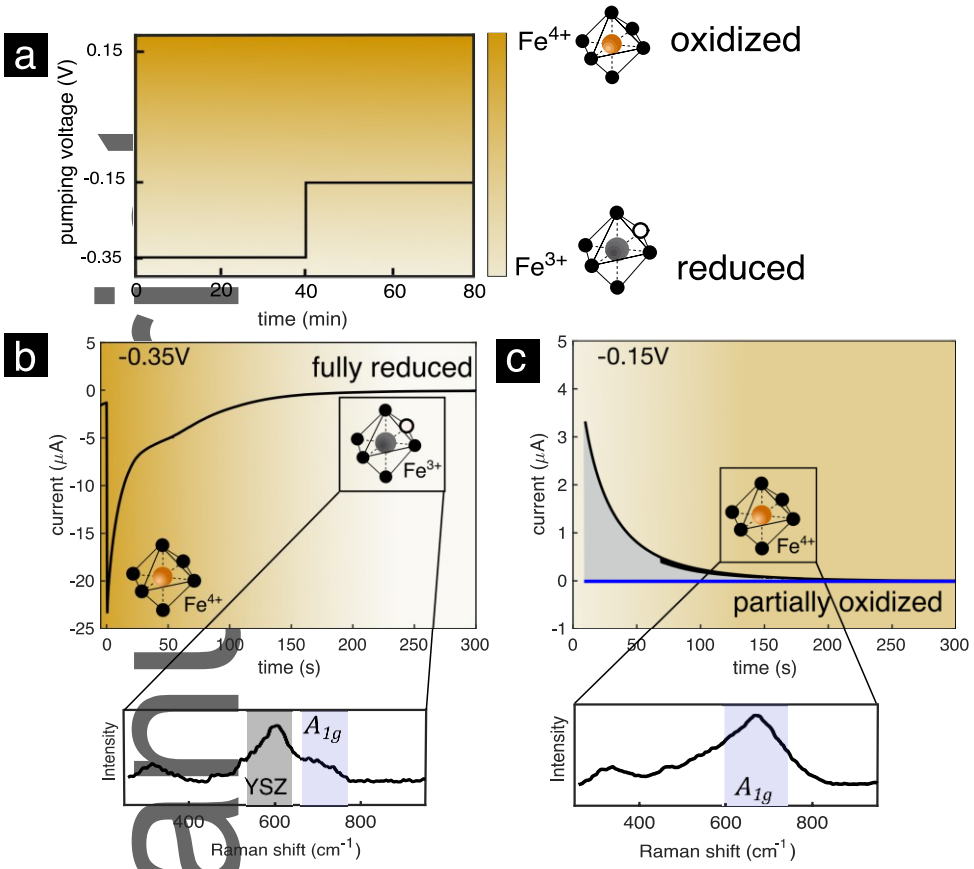

Figure 4: Example experimental procedure for the oxygen nonstoichiometry determination. a. Application of the pumping voltage over time. b. Reduction of the virgin $SrTi_{0.5}Fe_{0.5}O_{3-y}$ film at -0.35 V (vs. reference). Below is the Raman spectrum of the reduced $SrTi_{0.5}Fe_{0.5}O_{2.75}$ film. The enhanced peak belongs to the YSZ substrate. c. Subsequent oxidation at -0.15 V.The current due to pumping of oxygens into the $SrTi_{0.5}Fe_{0.5}O_{3-y}$ thin films is depicted in grey and the leakage current due to the exchange with the atmosphere is in blue. Below is the Raman spectrum taken after 40 min of applying -0.15 V. The oxygen stretching mode is highlighted.

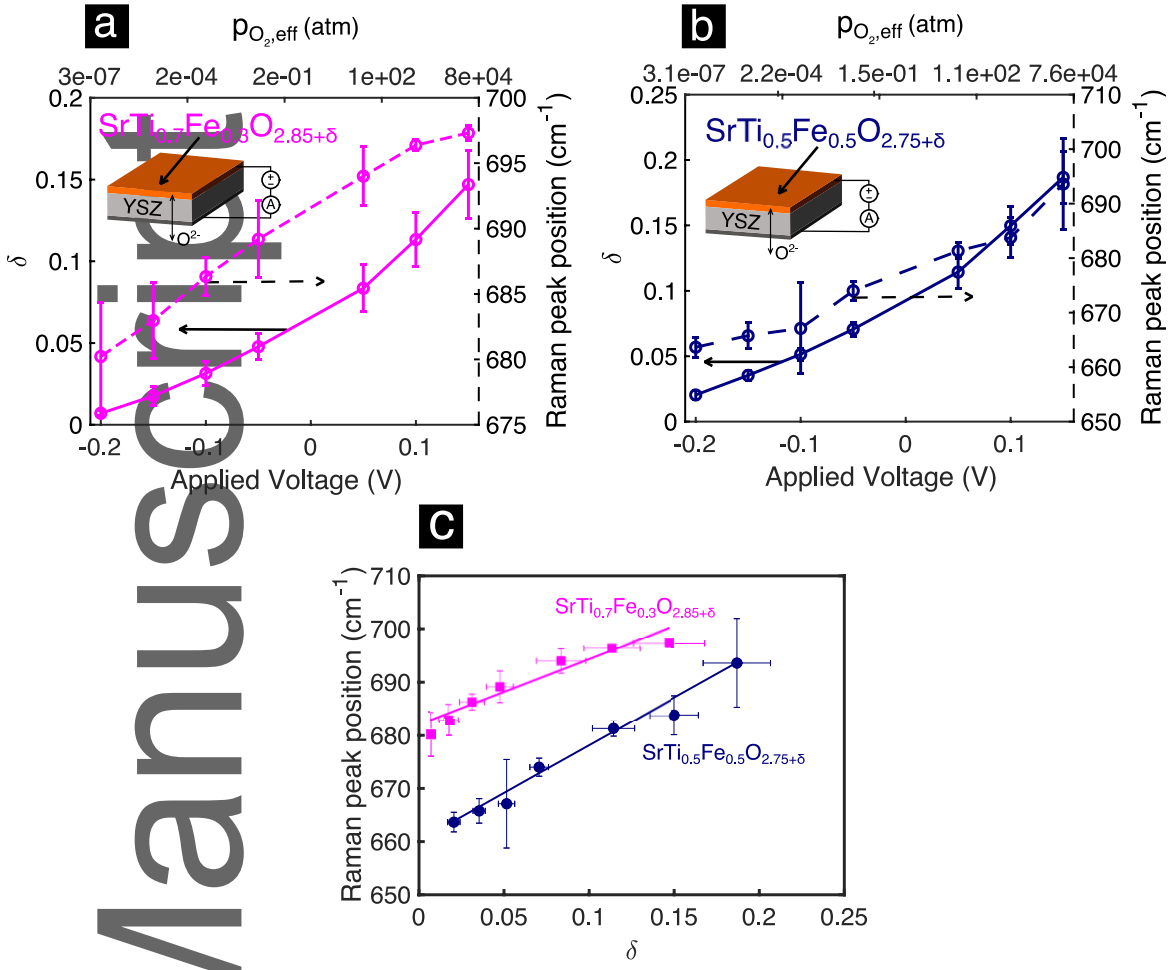

Figure 5: a.,b. Raman mode shift and oxygen nonstoichiometry as a function of the applied bias for 30 (a) and 50 mol% Fe (b). c. The Raman mode position as a function of the oxygen nonstoichiometry for both compositions.

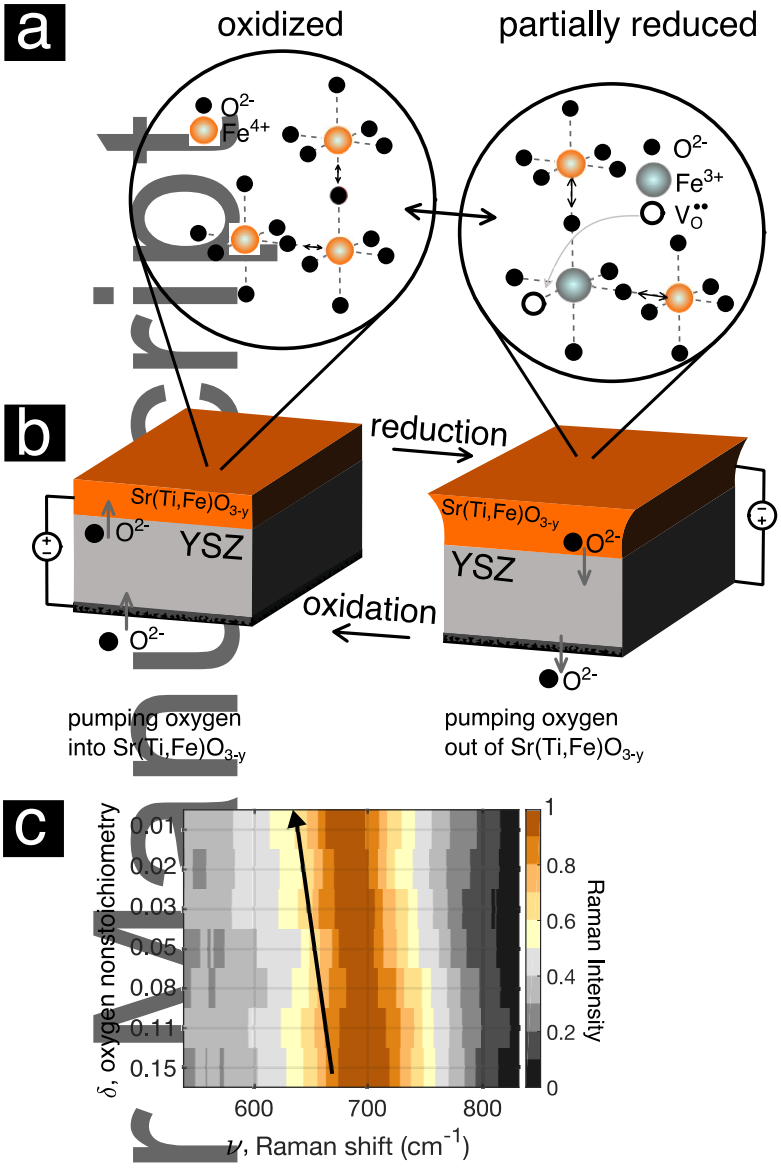

Figure 6: Summary of the mechanism of chemical expansion in the $Sr(Ti,Fe)O_{3-y}$ thin films integrated into the electrochemical cell with a YSZ electrolyte. a. Oxidation and reduction steps on the lattice level. b. Experimental set-up of the electrochemical cell with the chemical expansion of $Sr(Ti,Fe)O_{3-y}$ thin film in the reduced state highlighted. c. Intensity plot of the Raman spectra at various oxygen nonstoichiometry levels.

WILEY-VCH

Table of Content

ToC keyword: oxide perovskites

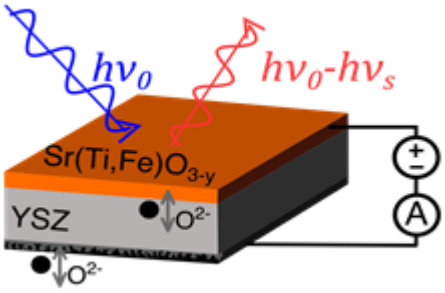

A new methodology is introduced on how to calibrate oxygen nonstoichiometry in perovskite thin films to their oxygen vibrational modes. This is achieved by actively pumping oxygen in and out of Sr(Ti,Fe)O_{3-y} thin films integrated into an electrochemical cell and measuring *in situ* Raman spectra.